Supporting Information

Trivalent Ions Mediated Abnormal Growth of All-Inorganic Perovskite Nanocrystals and the Divergent Emission Properties

Xunyi Dong[†a], Emmanuel Acheampong Tsiwah[†a], Tan Li[a], Junjie Hu[b], Zixiong Li[a], Yanxi Ding[a], Zhao Deng[c], Wenhui Chen[a], Like Xu[a], Peng Gao[*b], Xiujian Zhao[a], Yi Xie[*a]

[a] State Key Laboratory of Silicate Materials for Architectures, Wuhan University of Technology (WUT), No. 122, Luoshi Road, Wuhan 430070, P. R. China

[b] Laboratory of Advanced Functional Materials, Xiamen Institute of Rare-earth Materials, Chinese Academy of Science, No. 1300 Jimei Road, Jimei District, 361021, Xiamen, Fujian, P.R.China.

[c] State Key Laboratory of Advanced Technology for Materials Synthesis and Processing, Wuhan University of Technology, Wuhan, China

[†]*These authors contributed equally to this work.*

Email: xiey@whut.edu.cn; peng.gao@fjirsm.ac.cn

Contents

1. Characterization of perovskite $CsPbBr_3$ NC achieved by one-pot synthesis

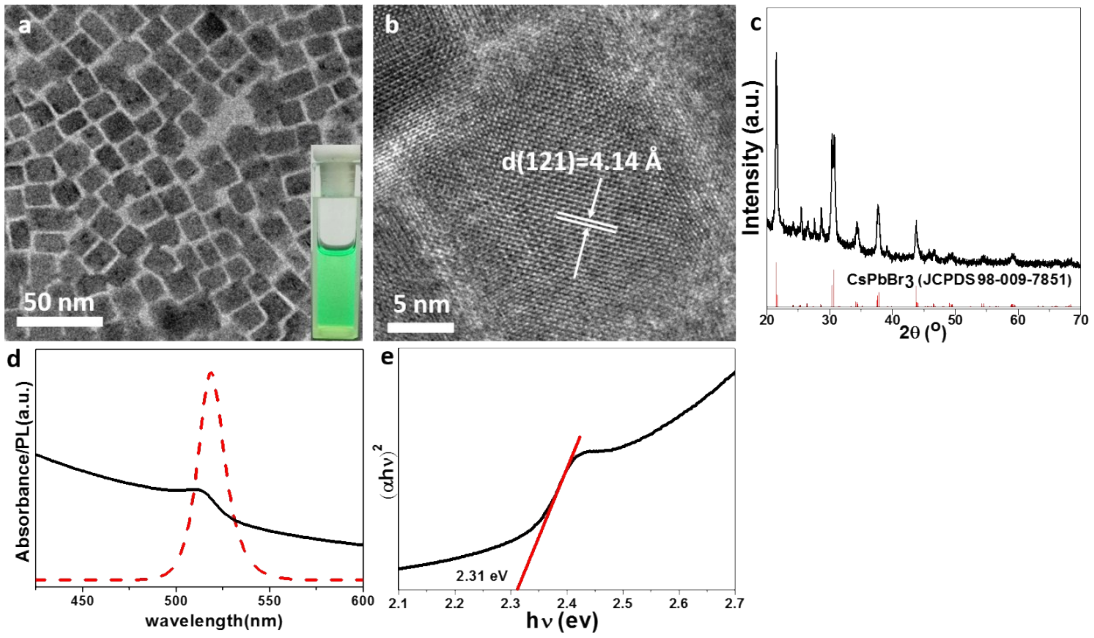

Fig. S1. *TEM (a) and HRTEM (b) images, XRD pattern (c), optical absorbance (black line) and PL emission (red line) spectra (d), and Tauc plot (e) of the $CsPbBr_3$ NCs achieved by one-pot synthesis under Ar atmosphere, in the absence of any foreign cations. Inset in panel a) presents the photograph of $CsPbBr_3$ NCs dispersed in hexane under UV light illumination (355 nm excitation wavelength).*

2. Characterization of the Bi-doped $CsPbBr_3$ NCs formed in the presence of $BiBr_3$

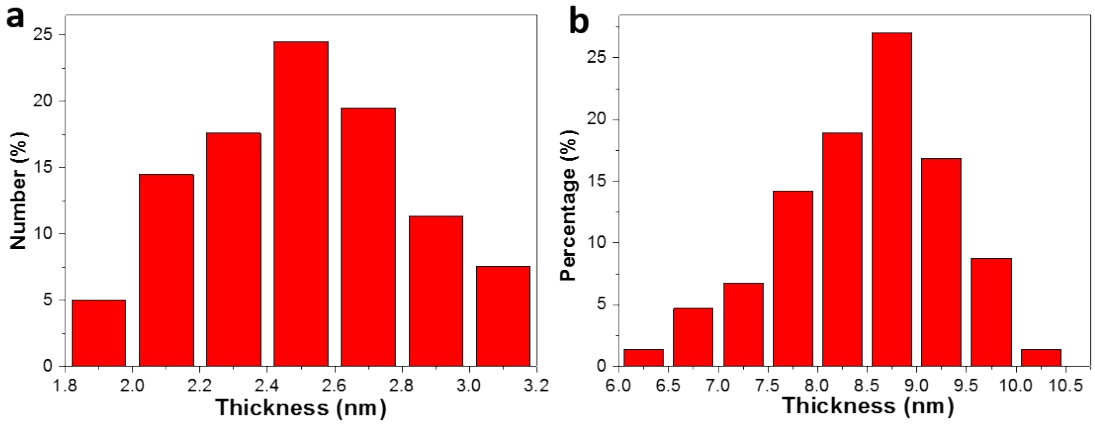

Fig. S2. *Size (in thickness) distribution histogram for the two NPL populations of $CsPbBr_3$ with different average thicknesses. The corresponding TEM images for the size calculation are from panels b) and c) of the Fig. 1 in the main text. The average thicknesses of the two NPLs populations are calculated to be 2.5 ± 0.3 nm, 8.5 ± 0.8 nm, respectively.*

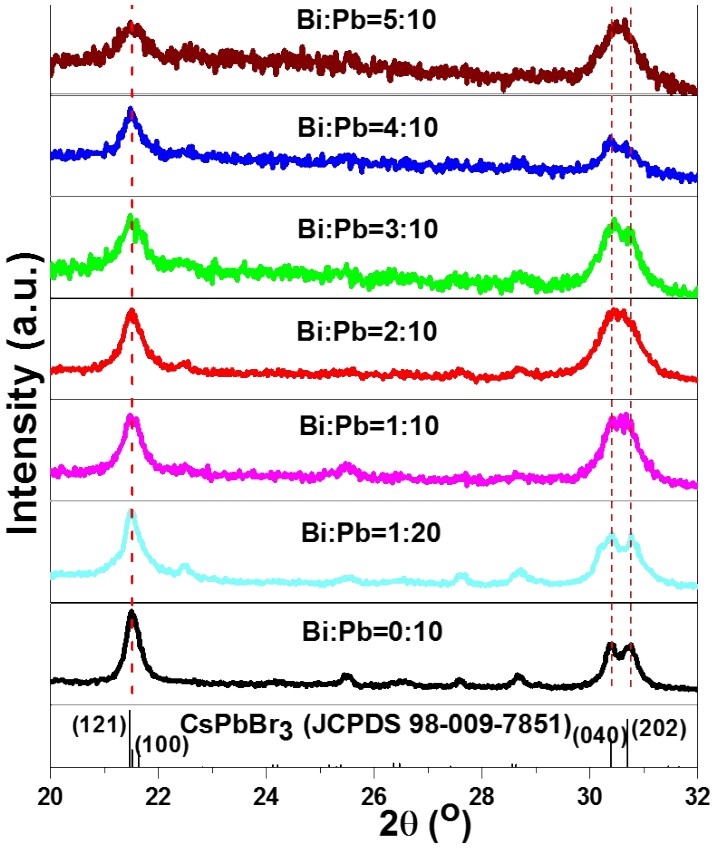

Fig. S3. *XRD patterns of the $CsPbBr_3$ NCs achieved with different precursor Bi:Pb ratios as dictated.*

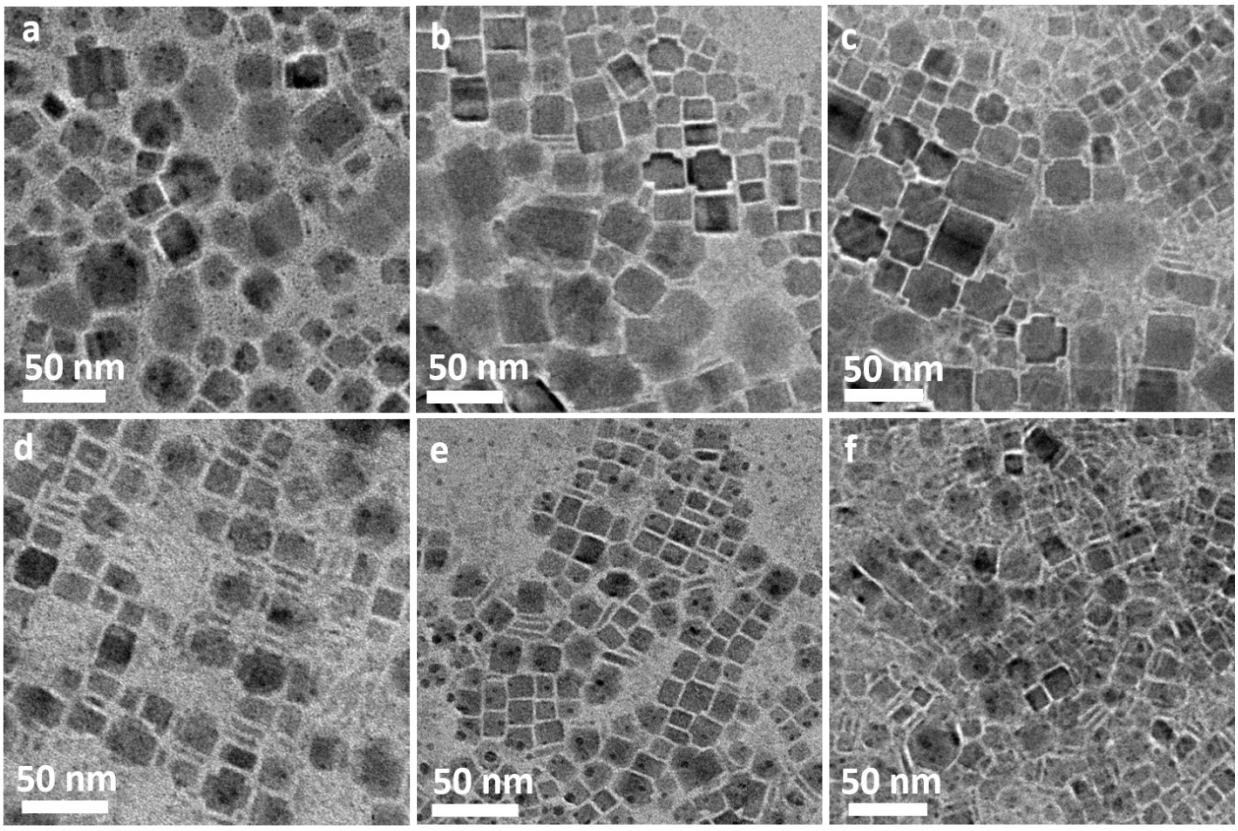

Fig. S4. *TEM images of the crude $CsPbBr_3$ perovskite NCs as-achieved with precursor Bi:Pb ratios of 1:20 (a), 1:10 (b), 2:10 (c), 3:10 (d), 4:10 (e) and 5:10 (f).*

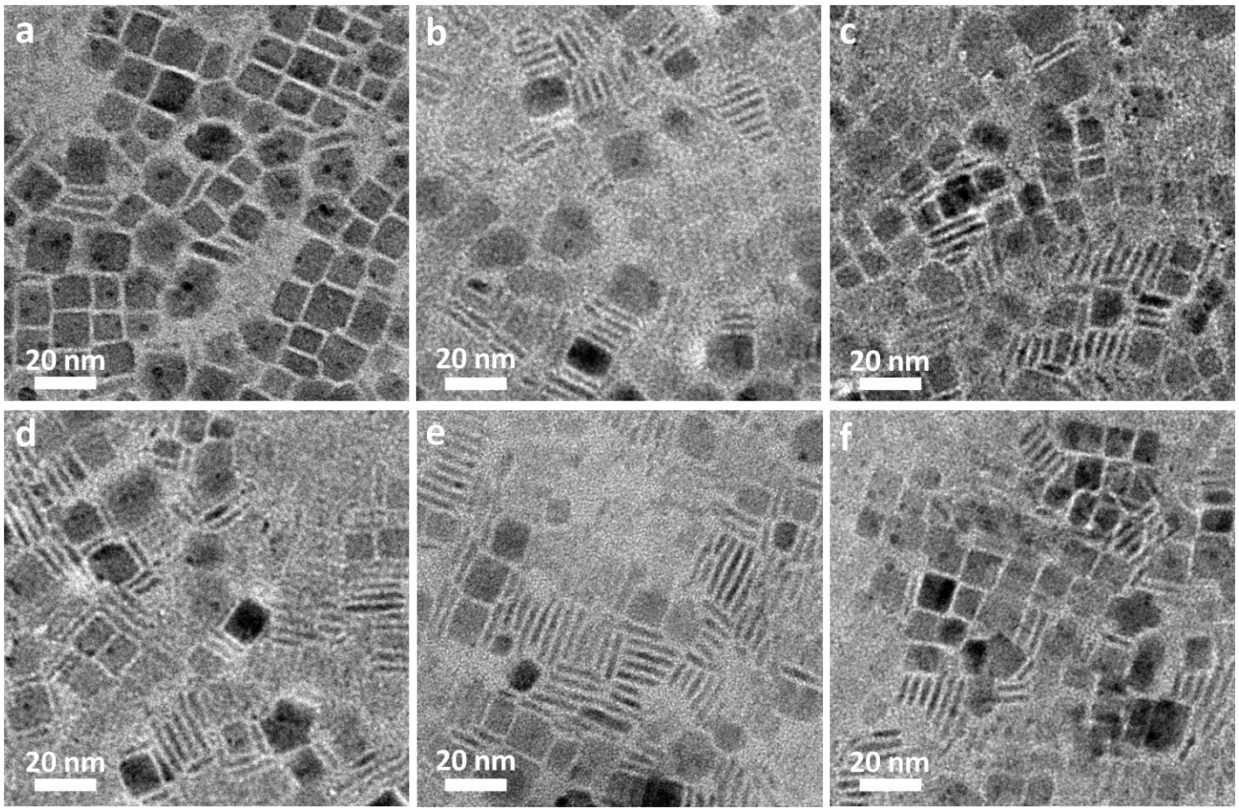

Fig. S5. *TEM images of the perovskite $CsPbBr_3$ NPLs with small thickness of ~2.5 nm. The NPLs were collected by centrifugation selection of the various samples as-formed with precursor Bi:Pb ratios of 1:20 (a), 1:10 (b), 2:10 (c), 3:10 (d), 4:10 (e) and 5:10 (f).*

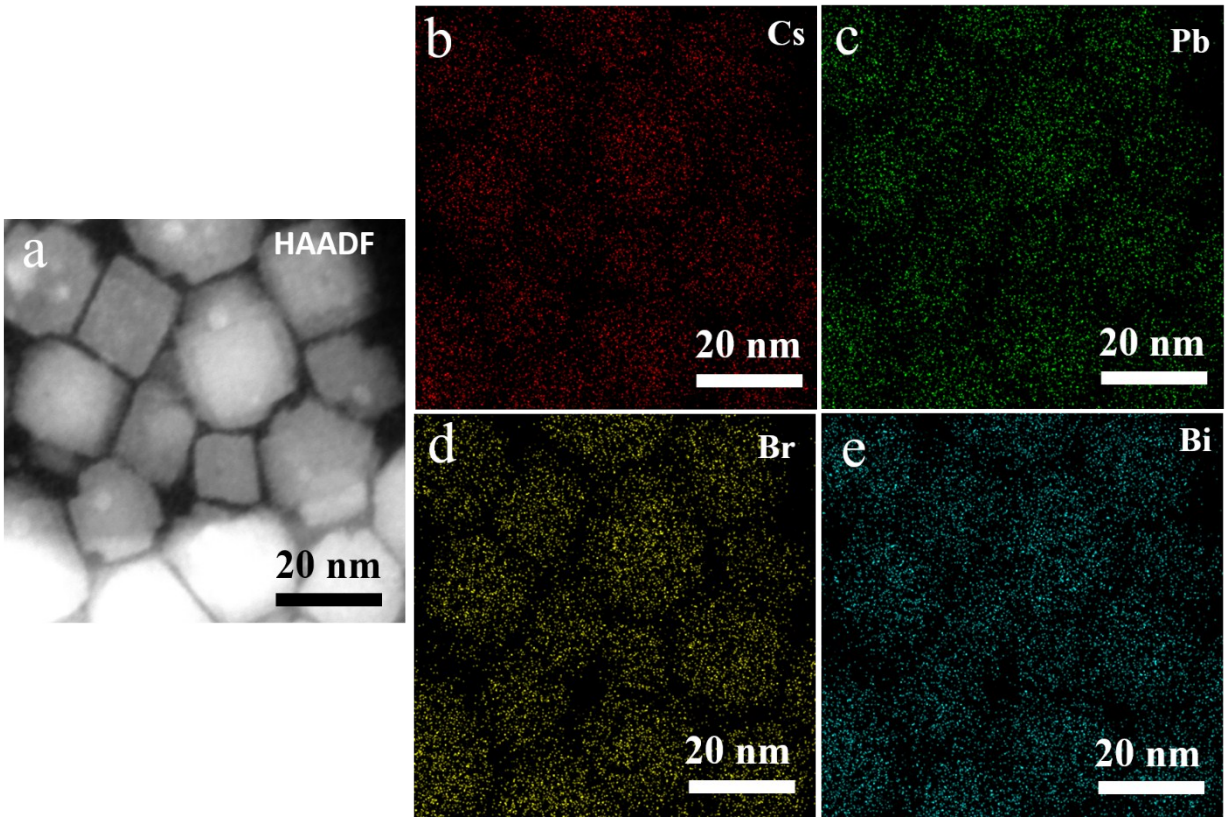

Fig. S6. *(a) HAADF-STEM image of the Bi-doped $CsPbBr_3$ NPLs with small thickness of ~2.5 nm, and the corresponding maps of (b) Cs, (c) Pb, (d) Br, and (e) Bi, demonstrating the presence of different elements in the Bi-doped perovskite NCs. The NPLs were collected by centrifugation selection.*

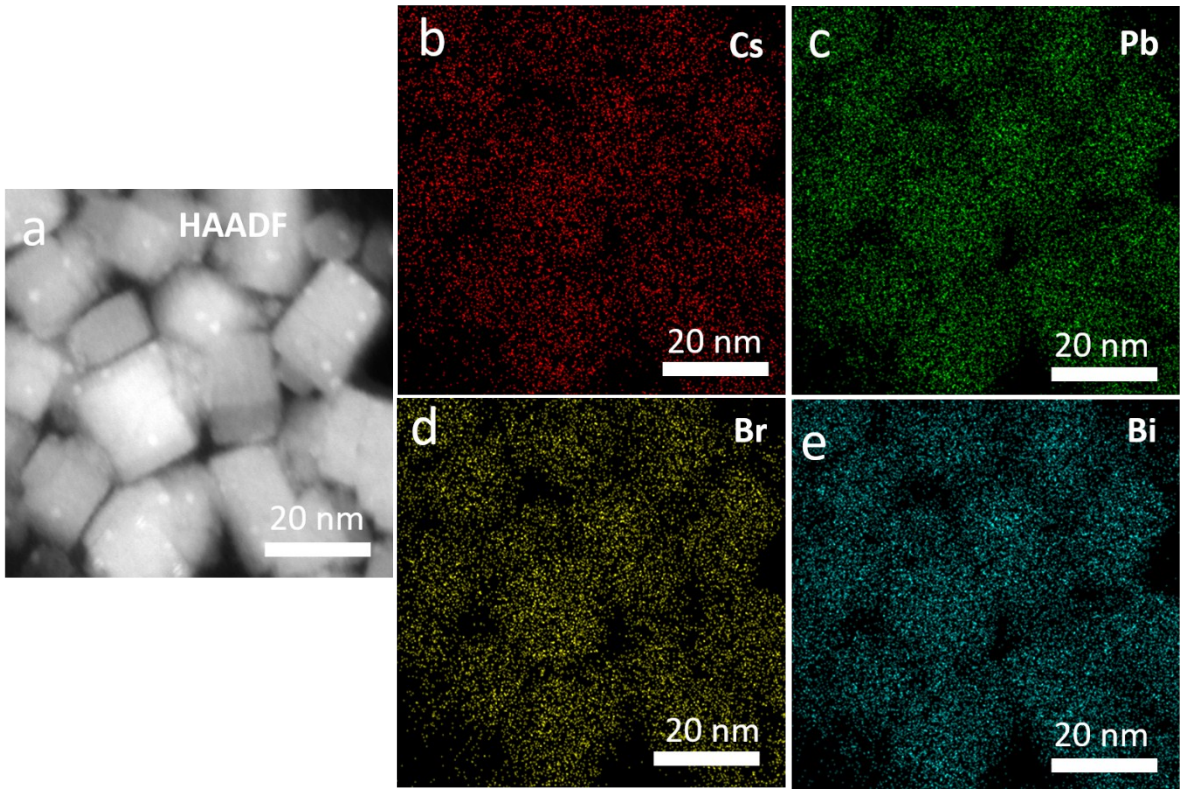

Fig. S7. *(a) HAADF-STEM image of the thick Bi-doped $CsPbBr_3$ NPLs collected by size selection and the corresponding maps of (b) Cs, (c) Pb, (d) Br, and (e) Bi, demonstrating the presence of different elements in the Bi-doped perovskite NCs.*

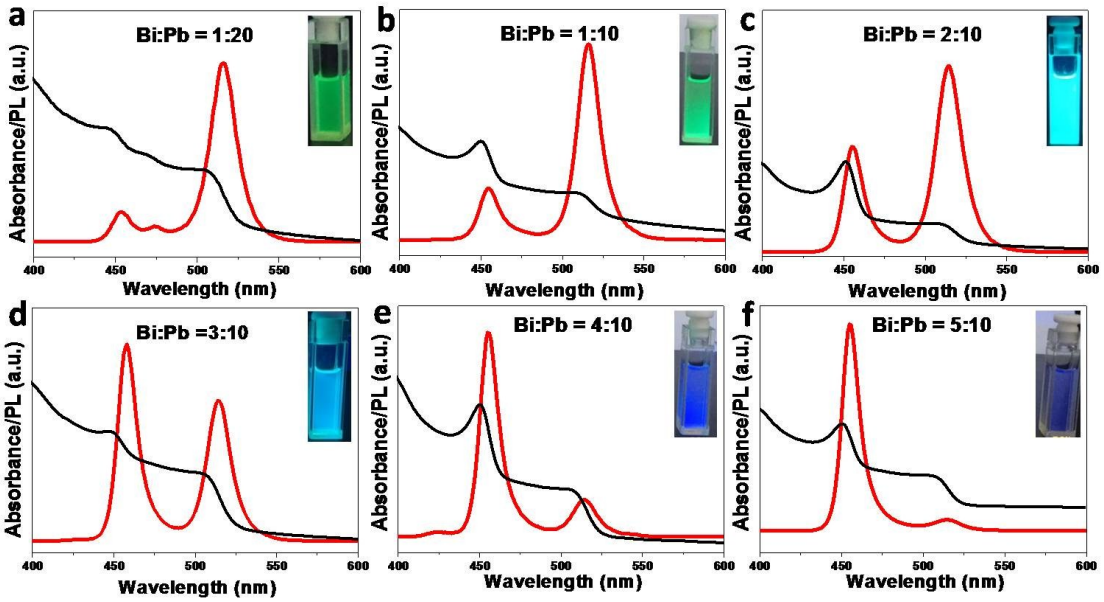

Fig. S8. *Optical absorbance (black lines) and PL spectra (red lines) of the various* $CsPbBr_3$ *NCs achieved with different precursor Bi:Pb ratios as dictated.*

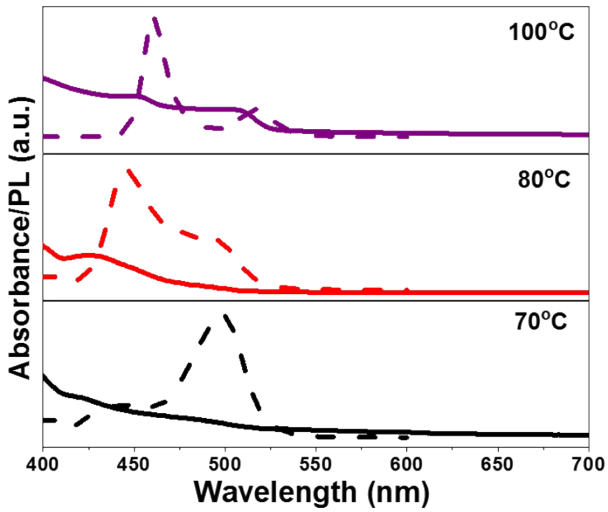

Fig. S9. *The steady-state absorption spectra (solid curves) and PL spectra (dash curves) of the aliquots collected at different temperatures during heating up. The samples are collected in the presence of* $BiBr_3$ *by fixing Bi:Pb as 4:10.*

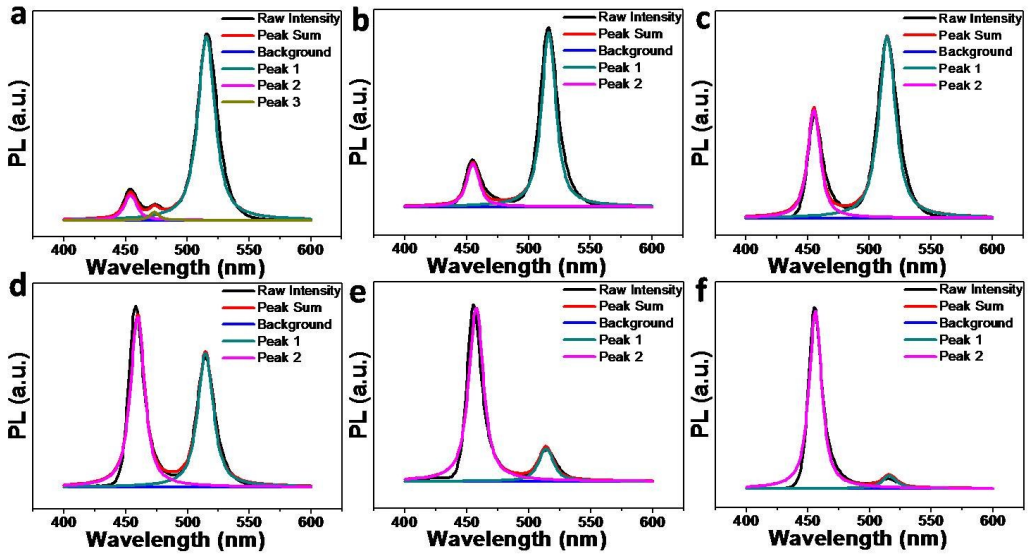

Fig. S10. *Multi-peak fitting of the PL spectra for the $CsPbBr_3$ NCs achieved with precursor Bi:Pb ratios of 1:20 (a), 1:10 (b), 2:10 (c), 3:10 (d), 4:10 (e) and 5:10 (f). The multi-peak-emitting spectra were fitted by the type of Gaussian. The peak positions extracted from the fit are listed in Table S1. The results indicate that the as-synthesized samples consist of NPLs with different sized (in thickness).*

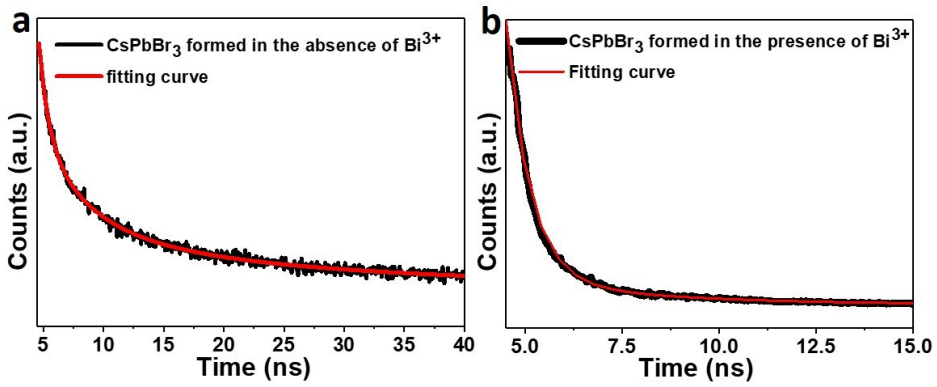

Fig. S11. *Time-resolved PL decay spectra (excitation at 510 nm) and the corresponding fitted curves of the $CsPbBr_3$ NCs in the absence (a) and presence (b) of Bi^{3+}, respectively. PL decay curves were well fitted with tri-exponential function.*

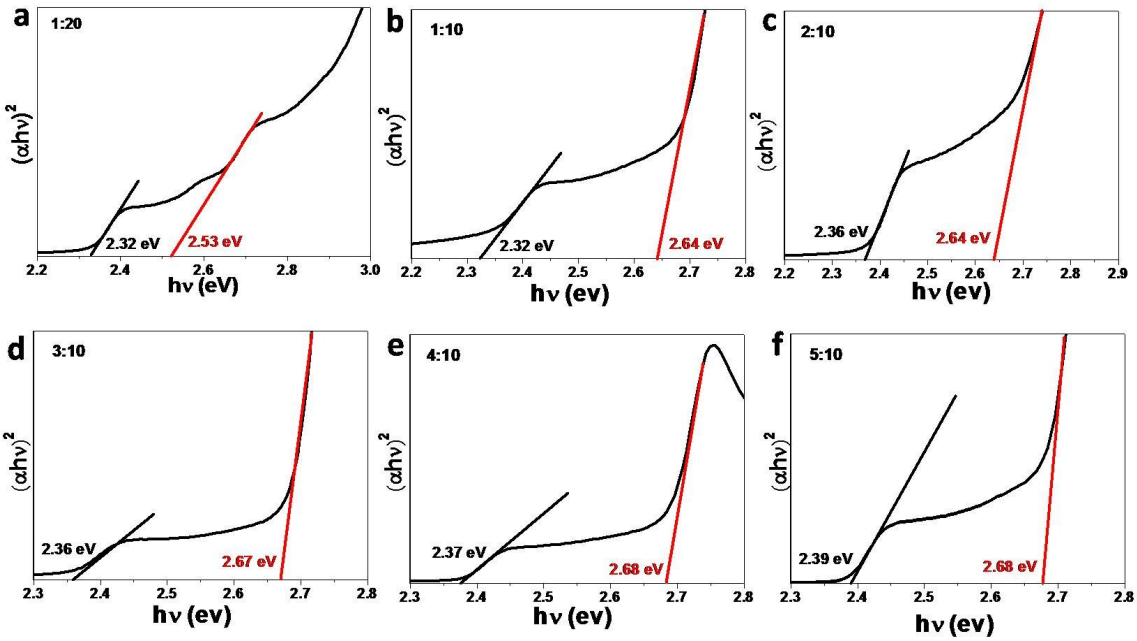

Fig. S12. *Tauc plots of undoped $CsPbBr_3$ NCs (a) and $CsPbBr_3$ NCs formed in the presence of different amount of Bi^{3+} ions in the precursor (labelled as feed Bi:Pb ratio) as dictated.*

Table S1. *The summarization on the optical characterization of the $CsPbBr_3$ NCs achieved in the presence of different amount of Bi^{3+} ions in the precursor (labelled as feed Bi:Pb ratio). The band gaps (Eg) are estimated from Tauc formula.*

Feed Bi:Pb ratio	Dual PL peaks[a] (nm)		Eg (eV)		FWHM[b] (nm)		Final Bi:Pb ratio (found by ICP)
	Peak1	Peak2	Peak1	Peak2	Peak1	Peak2	
0:10	518.6		2.31		17.31		0%
1:20	515.4	454.0	2.32	2.53	16.50	12.00	0.8%
1:10	516.2	455.0	2.32	2.64	13.60	12.00	3.0%

2:10	514.4	455.0	2.36	2.64	16.00	12.20	4.9%
3:10	514.3	458.4	2.36	2.67	15.00	13.00	7.2%
4:10	513.9	457.5	2.37	2.68	14.00	14.00	10.8%
5:10	515.0	456.1	2.39	2.68	15.00	12.30	13.7%

[a] Dual PL peaks after deconvolution.

[b] Full width at half-maximum (FWHM) of each PL peak after deconvolution.

Table S2. *Photoluminesence quantum yields (PLQY) of the typical perovskite NCs. The Bi:Pb ratio in the precursor is 2:10.*

Samples	Bi:Pb (%, found by ICP)	PLQY (%)
$CsPbBr_3$ formed in the absence of Bi	0	19.67
$CsPbBr_3$ formed in the presence of $BiBr_3$	4.9	43.96
$CsPbCl_xBr_{3-x}$ formed in the presence of $BiCl_3$	4.9	9.52

Table S3. *Final Bi:Pb ratio of the typical thin NPLs groups and thick particles upon centrifugation at low centrifugal velocity.*

Feed Bi:Pb ratio	Groups of particles	Final Bi:Pb ratio (found by ICP)	Final Bi:Pb ratio (found by EDS)
3:10	Thin NPLs	8.3:100	6.9:100
	Thick particles	7.0:100	6.3:100

3. Characterization of the $CsPbBr_3$ NCs achieved in the presence of $BiFeO_3$

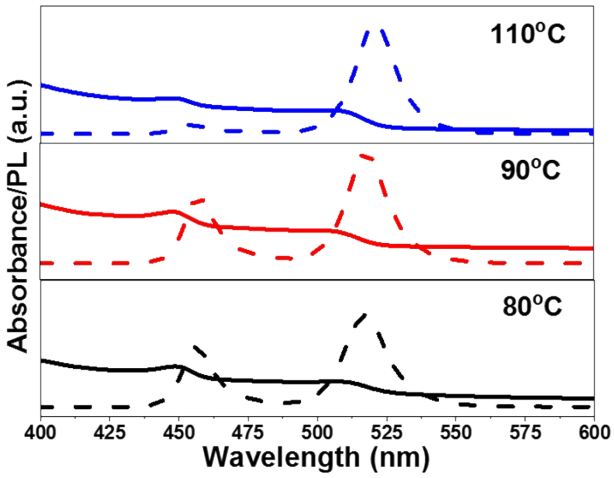

Fig. S13. *Optical absorbance spectra (solid curves) and PL spectra (dash curves) of the various $CsPbBr_3$ aliquots collected at different temperatures as dictated. The $CsPbBr_3$ NCs achieved in the presence of $BiFeO_3$.*

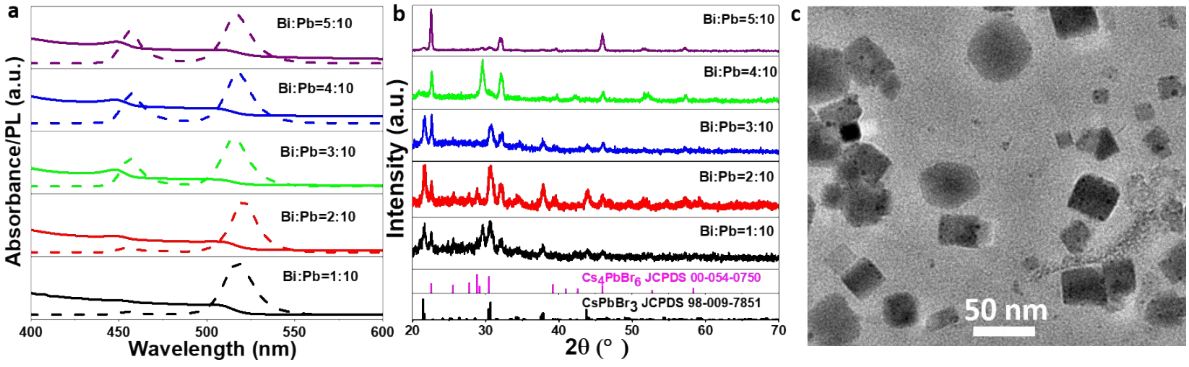

Fig. S14. *(a) Optical absorbance spectra (solid curves) and PL spectra (dash curves), (b) XRD patterns of the various $CsPbBr_3$ NCs collected with different precursor Bi:Pb ratios as dictated. (c) TEM image of the typical NCs collected by fixing precursor Bi:Pb = 3:10. The NCs were achieved in the presence of $BiFeO_3$. XRD patterns indicate mixed phases in the resulting samples. TEM image suggests that the NCs are not uniform in morphology.*

4. Characterization of the $CsPbBr_3$ NCs achieved in the presence of Al^{3+} ions

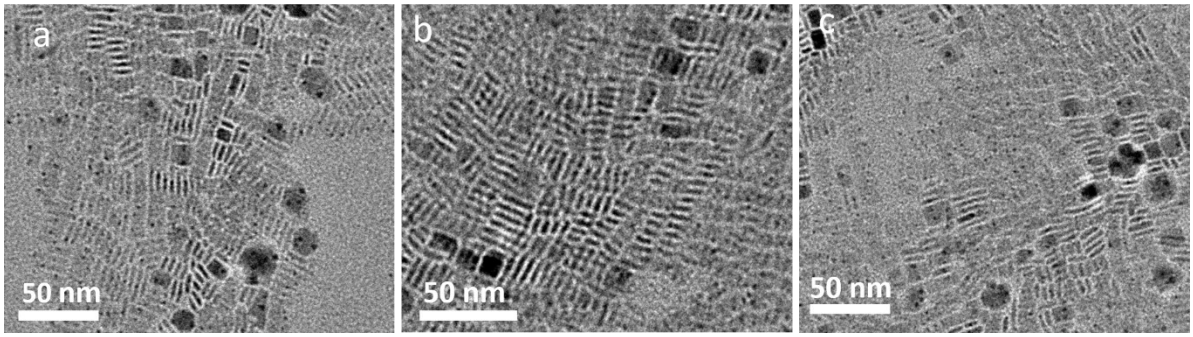

Fig. S15. *TEM images of the $CsPbBr_3$ NPLs collected in the presence of $AlBr_3$ in the precursor by fixing Al:Pb ratios of 1:10 (a), 2:10 (b) and 3:10 (c), respectively.*

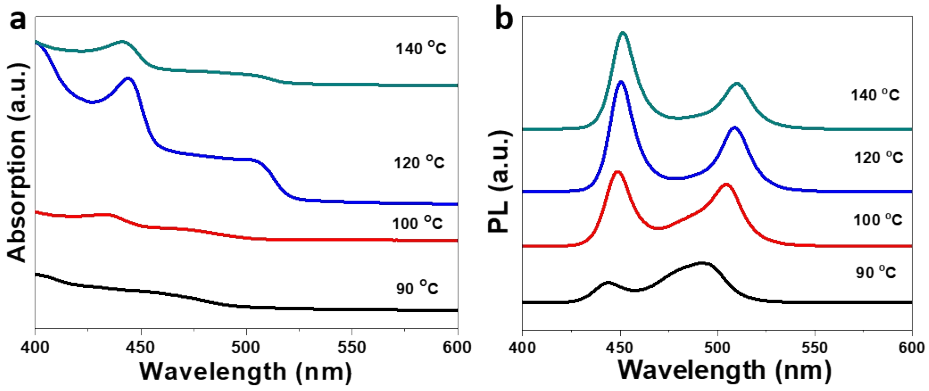

Fig. S16. *Optical absorbance spectra (a) and PL spectra (b) and XRD patterns of the $CsPbBr_3$ NCs collected at different temperatures as dictated, in the presence of $AlBr_3$ by fixing Al:Pb ratios of 3:10.*

5. Characterization of the $CsPbBr_3$ NCs achieved in the presence of In^{3+} ions

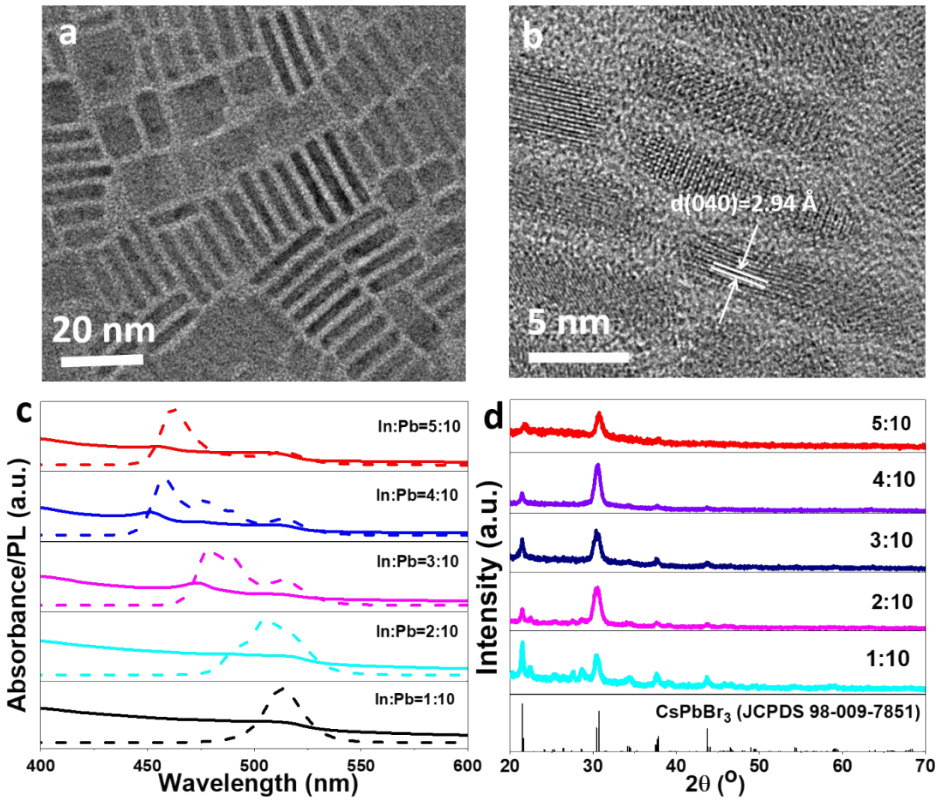

Fig. S17. *(a-b) TEM (a) and HRTEM (b) images of the typical $CsPbBr_3$ NPLs synthesized in the presence of $InBr_3$. (c-d) Optical absorbance spectra and PL spectra (c) and XRD patterns (d) of various $CsPbBr_3$ NCs collected in the presence of different precursor In:Pb ratios as dictated.*

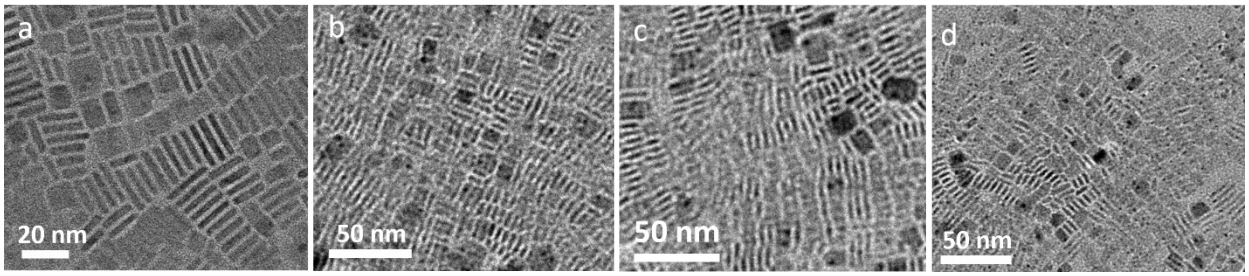

Fig. S18. *TEM images of the $CsPbBr_3$ NPLs collected in the presence of $InBr_3$ by fixing In:Pb ratios of 1:10 (a), 2:10 (b) 3:10 (c) and 5:10 (d), respectively.*

6. Characterizations of the $CsPbCl_xBr_{3-x}$ NCs achieved in the presence of $BiCl_3$

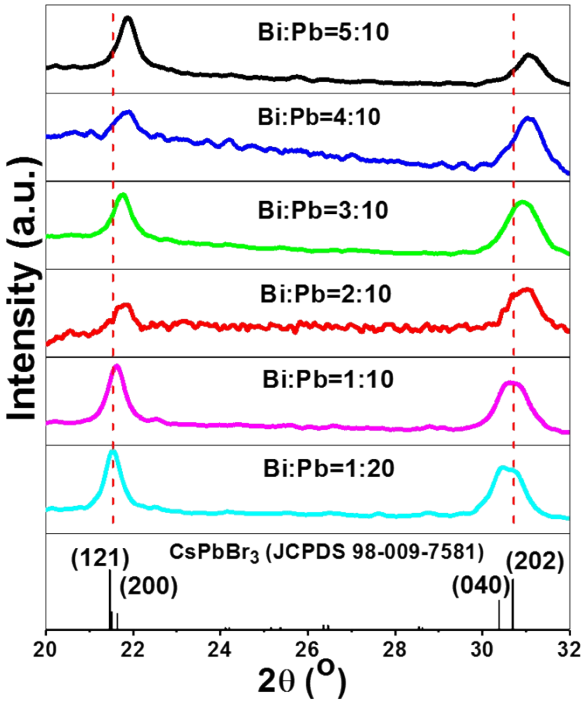

Fig. S19. *XRD patterns of the $CsPbCl_xBr_{3-x}$ NCs achieved with different precursor Bi:Pb ratios as dictated. The samples were prepared in the presence of $BiCl_3$.*

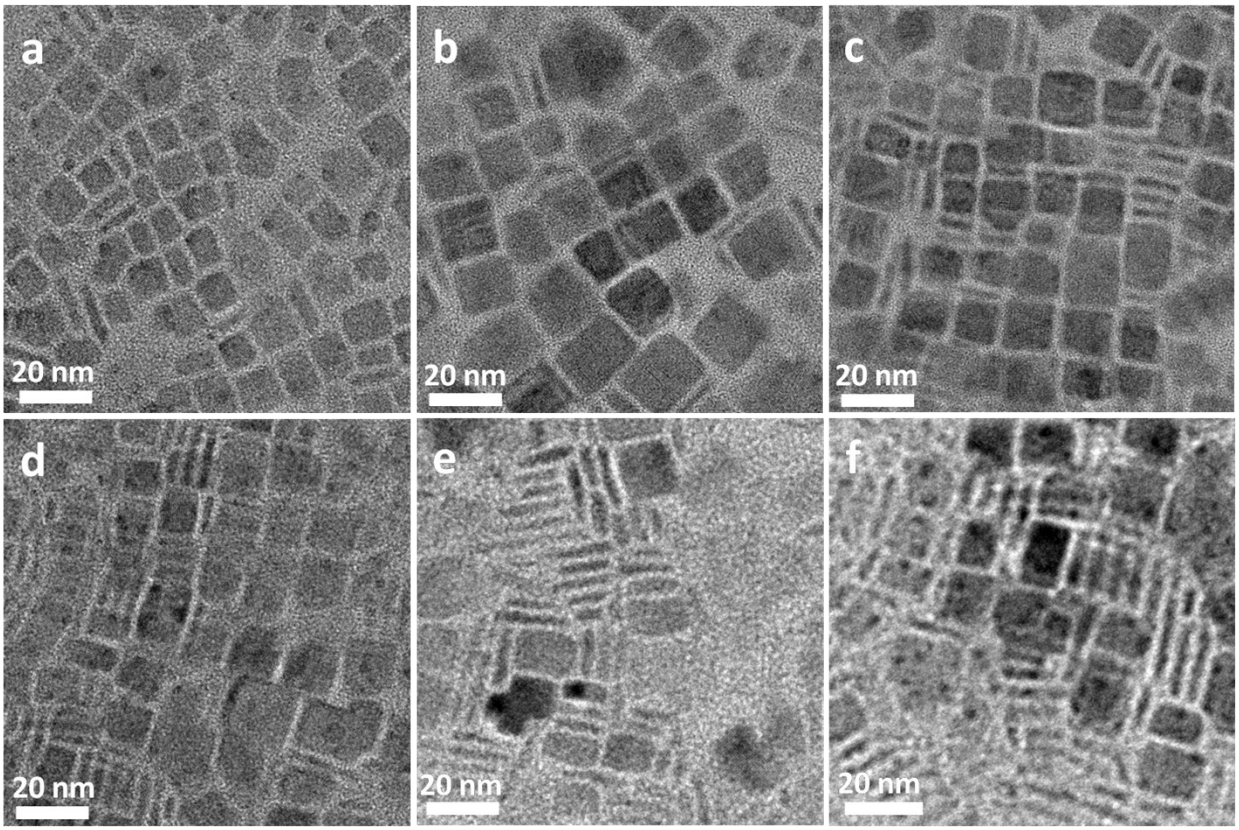

Fig. S20. *TEM images of the perovskite $CsPbCl_xBr_{3-x}$ NPLs, which were collected from the top solution upon centrifugation selection of the various samples as-formed in the presence of precursor Bi:Pb ratios of 1:20 (a), 1:10 (b), 2:10 (c), 3:10 (d), 4:10 (e) and 5:10 (f). The samples were prepared in the presence of $BiCl_3$.*

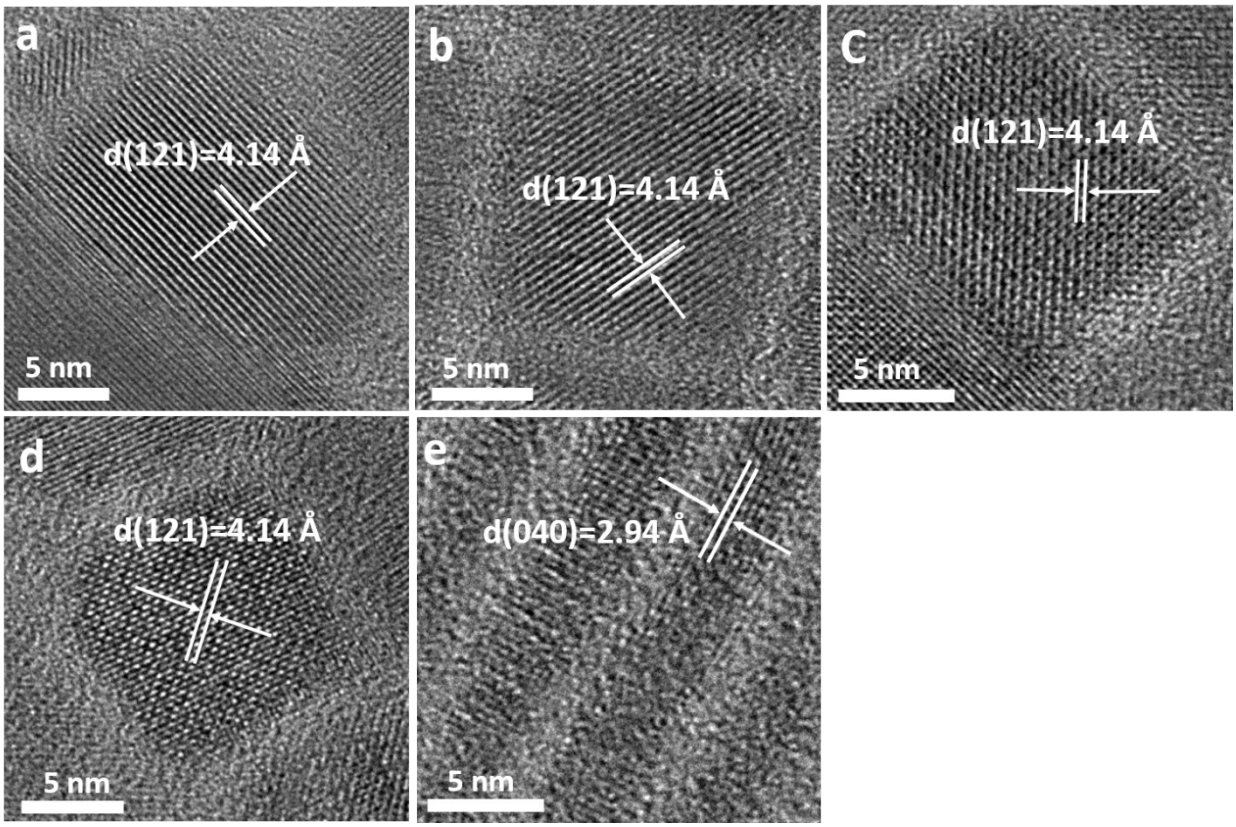

Fig. S21. *(a-d) Top-view of HRTEM images of the representative individual perovskite $CsPbBr_3$ NPLs with average thickness of around 2.5 nm, which were achieved in the presence of precursor Bi:Pb ratios of 1:20 (a), 1:10 (a), 2:10 (b), 3:10 (c), and 4:10 (d). (e) side-view of HRTEM image of the individual perovskite $CsPbBr_3$ NPLs achieved with precursor Bi:Pb ratio of 2:10.*

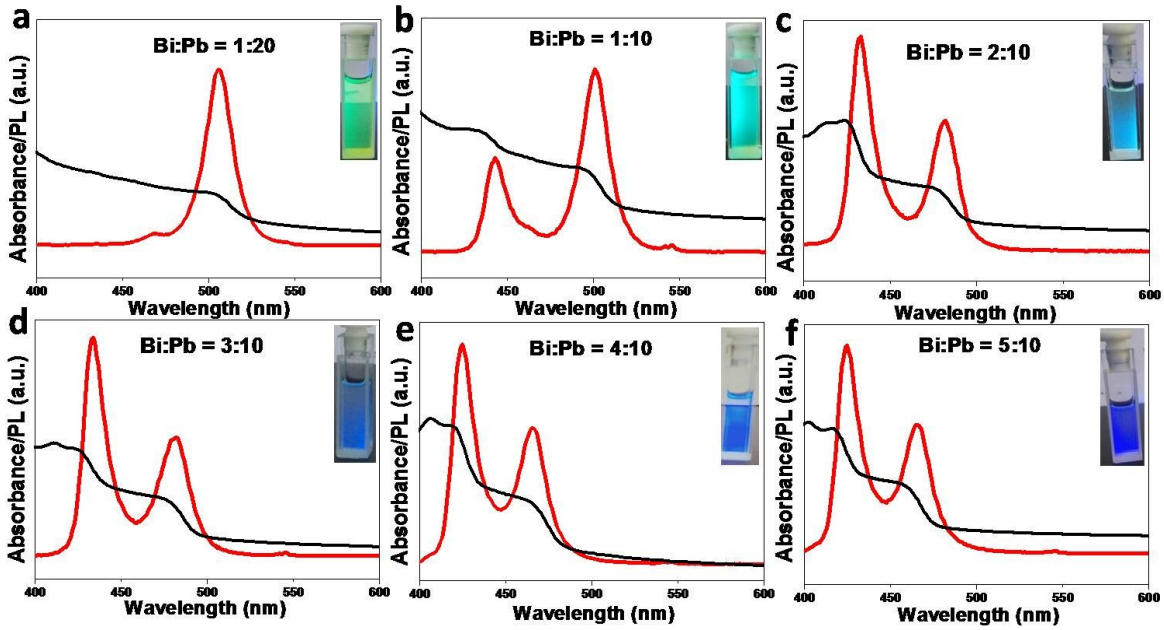

Fig. S22. *Optical absorbance (black lines) and PL spectra (red lines) of the* $CsPbCl_xBr_{3-x}$ *NCs achieved with different precursor Bi:Pb ratios as dictated. Insets in each panel present the photographs of corresponding NCs dispersed in hexane under UV light illumination (355 nm excitation wavelength).*

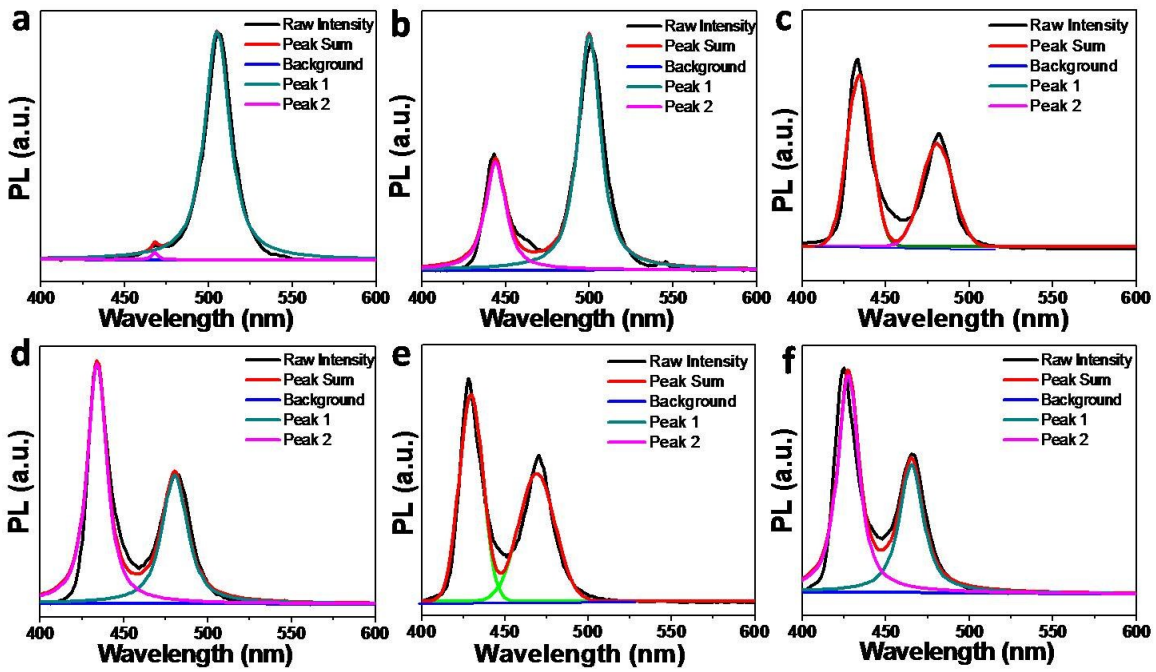

Fig. S23. *Deconvolution of the PL spectra collected on the $CsPbCl_xBr_{3-x}$ NCs achieved with precursor Bi:Pb ratios of 1:20 (a), 1:10 (b), 2:10 (c), 3:10 (d), 4:10 (e) and 5:10 (f). For data fitting, a doublet was used for each PL spectrum.*

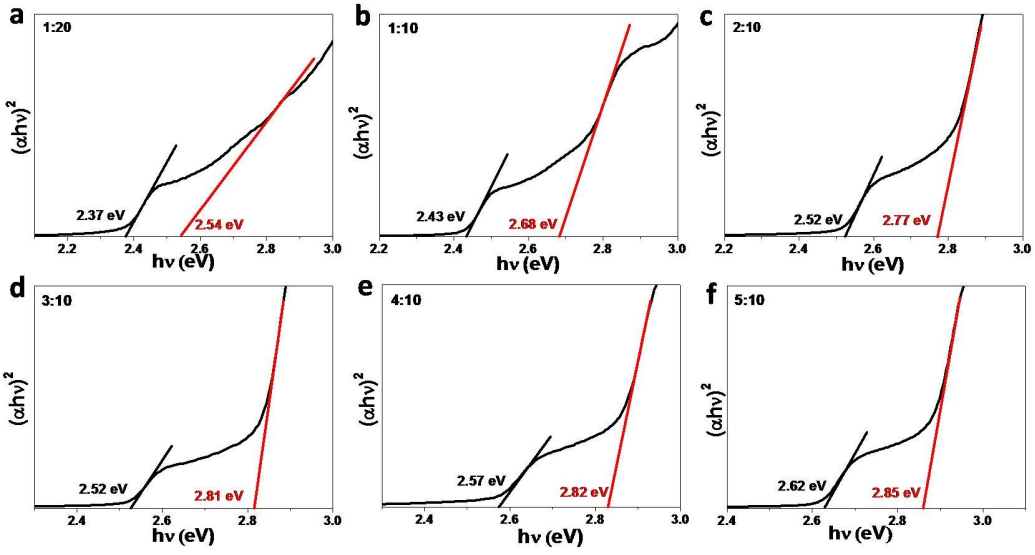

Fig. S24*. Tauc plots of the $CsPbCl_xBr_{3-x}$ NCs formed in the presence of different precursor Bi:Pb ratios as dictated.*

Table S4. *The summarization on the optical characterization of the* $CsPbCl_{3-x}Br_3$ *NCs achieved in the presence of different Bi:Pb precursor ratios.*

Feed Bi:Pb ratio	Dual PL peaks[a] (nm)		Band gap (eV) from Tauc formula		FWHM[b] (nm)		Final Bi:Pb ratio (found by ICP)
	Peak1	Peak2	Peak1	Peak2	Peak1	Peak2	
1:20	505.1	467.9	2.37	2.54	18.00	4.75	1.3%
1:10	500.0	444.0	2.43	2.68	16.00	14.50	2.1%
2:10	480.7	434.2	2.52	2.77	18.00	14.00	2.6%
3:10	469.0	429.6	2.52	2.81	20.00	14.30	4.9%
4:10	565.3	427.5	2.57	2.82	17.00	15.00	7.7%
5:10	465.0	425.0	2.62	2.85	16.00	14.00	7.9%

[a] Dual PL peaks after deconvolution.

[b] Full width at half-maximum of the dual PL peaks after deconvolution.

7. XPS analyses of the typical Bi-doped $CsPbBr_3$ NCs

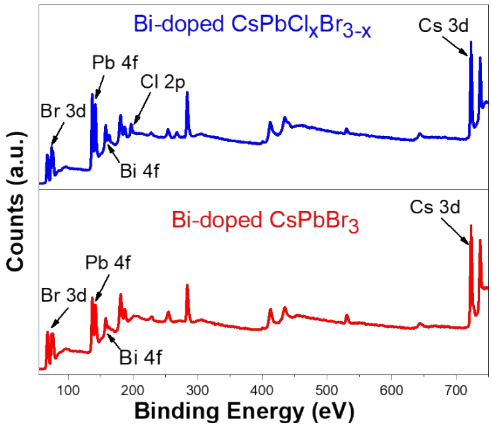

Fig. S25. *Survey XPS spectra of the typical Bi-doped NCs as dictated. It is noteworthy that Bi signal can be detected in all the doped NCs. XPS analyses further confirm that the elemental composition of the doped* $CsPbBr_3$ *and* $CsPbCl_xBr_{3-x}$ *NCs contains Cs, Pb, Bi and Br.*

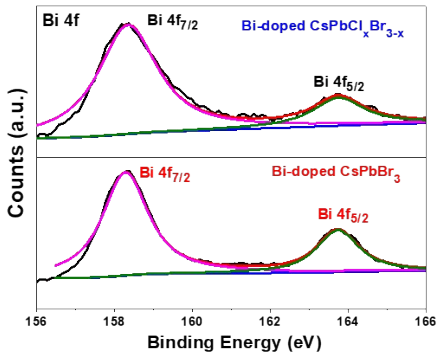

Fig. S26. *Deconvolution of the Bi 4f high-resolution XPS signals collected on the Bi-doped perovskite* $CsPbBr_3$ *and* $CsPbCl_xBr_{3-x}$ *NCs formed in the presence of* $BiBr_3$ *and* $BiCl_3$*, respectively.*

8. Details of computation

The density functional theory calculations were performed with the Vienna Ab-initio Simulation Package (VASP). The functional of choice was PBE. The inner electrons were represented by projector-augmented wave pseudopotentials (PAW), and the monoelectronic states were expanded in plane waves with a kinetic energy cutoff of 400 eV. Perovskite surfaces were modeled by a multi-layers slab and at least p(3 × 3) supercells, where the two uppermost layers were fully relaxed and the rest fixed to the bulk distances. In the surface calculations, the Brillouin zone was sampled by a Γ-centered k points mesh from the Monkhorst-Pack method, and the k point samplings were denser than 30 $Å^{-1}$. The vacuum between the slabs was at least 9 Å. and the adsorbates were placed only on one side of the slab, and thus adipole correction was applied to remove spurious contributions arising from this asymmetry. In all cases, the optimization thresholds were 10^{-5} eV and 0.02 eV $Å^{-1}$ for electronic and ionic relaxations, respectively.

Table S5. *The DFT surface energy relative parameters of the (010), (110) and (111) planes of* $CsPbBr_3$.

$CsPbBr_3$	(010)	(110)	(111)
E_{slab}: slab energy	- 286.9825	- 266.0951	- 267.3768
N:atoms	135	135	135
A: surface area	309.3342	460.8569	564.4314
γ: surface energy	0.01960	0.05846	0.04546

[a]per atom energy (E_{bulk}) in bulk is 2.1706 eV through the DFT calculations of the bulk $CsPbBr_3$.

Table S6. *The DFT slab energy (E_{slab}) and adsorption energy (E_a) about the slab models in the Fig. 3b and 3d.*

$CsPbBr_3$(010)	Slab energy	adsorption energy
Bi-Bi/(010) ortho	-289.8214	2.1468
Bi-Bi/(010) meta	-293.7857	- 1.8175
Bi/(010)	-288.0296	2.8029
Bi-Pb/(010)	-293.0987	- 1.2247

[a]DFT-based Bisumth absorption energy is calculated by E(Bi/surface) – E(Bi atom) – E(surface), and that of Lead by E(Pb/surface) – E(Pb atom) –E(surface); at first, we calculated the slab energy of one Bi atom on $CsPbBr_3$(010), then the slab energy in Table S5 was used to evaluate adsorption energy after one Bi atom adsorbed on $CsPbBr_3$(010) surface.

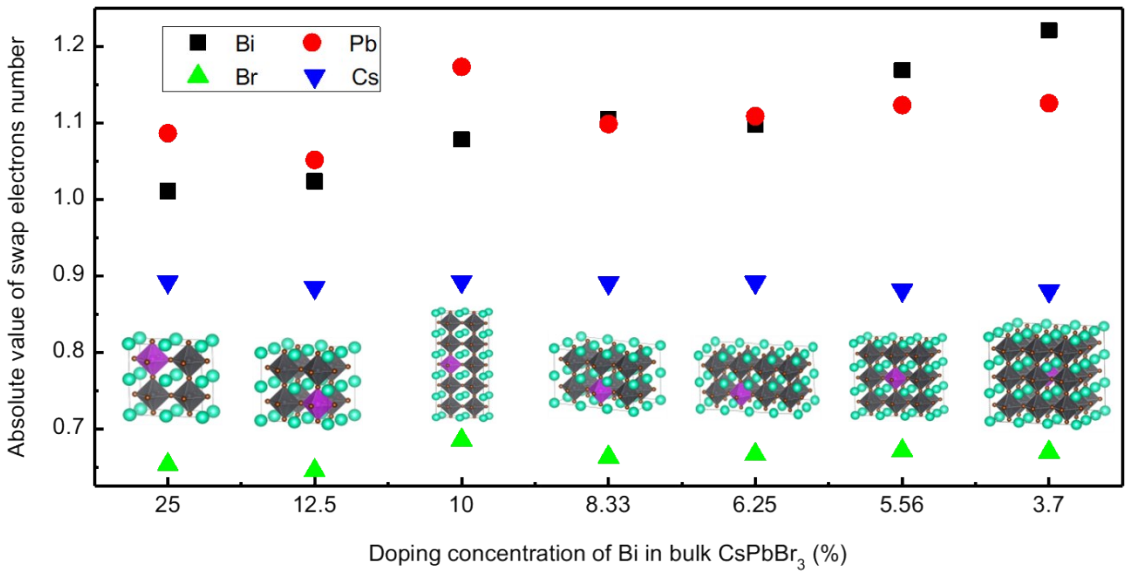

Fig. S27. *Calculation of absolute values of swap electron number for Bi doped $CsPbBr_3$ in different super cells based on the Bader's analysis theory.*

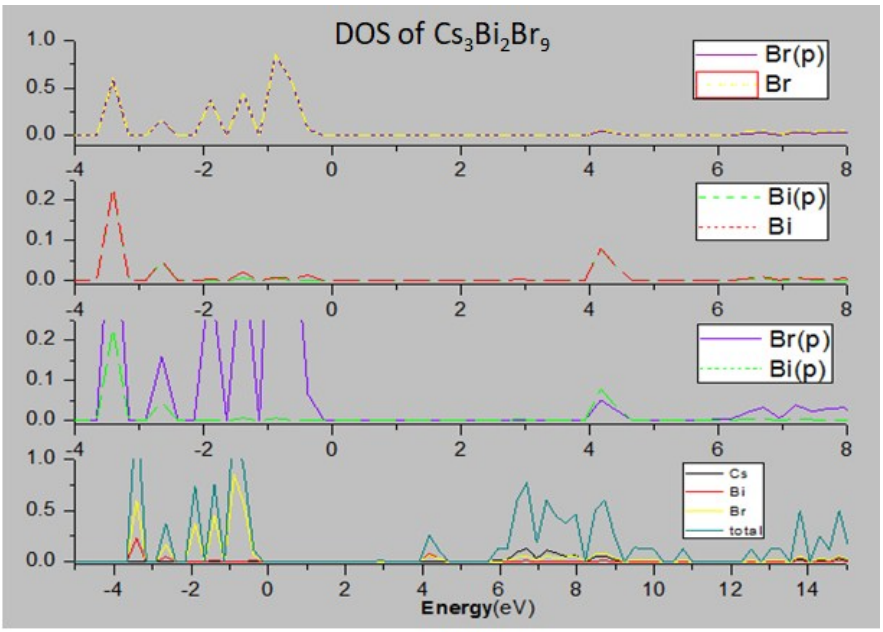

(a)

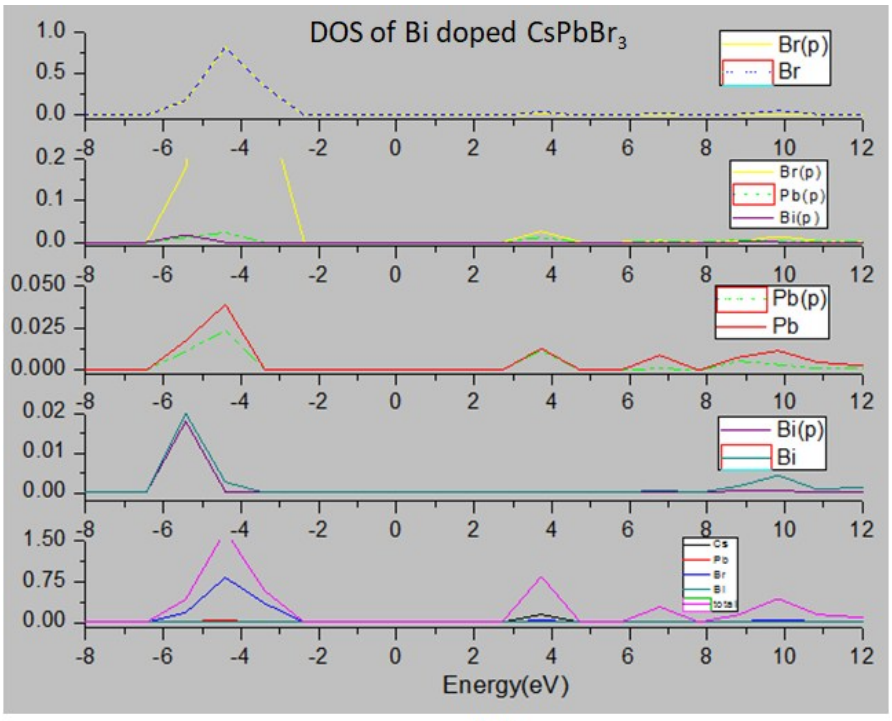

(b)

Fig. S28. *The density of states of $Cs_3Bi_2Br_9$ and projected density of states of per atom (a), and the density of states of supposed Bi doped the bulk $CsPbBr_3$ (b).*

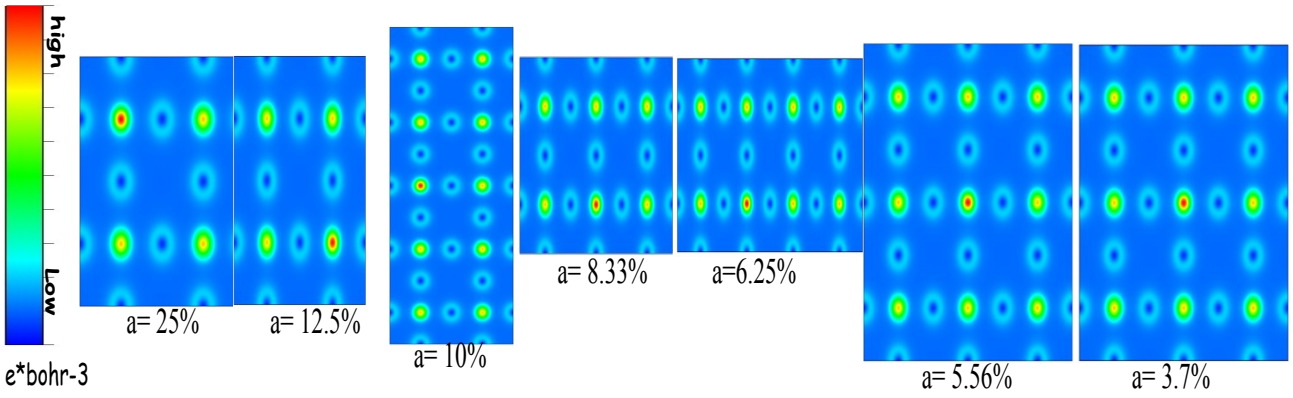

Fig. S29. *The charge density of Bi doped the bulk $CsPbBr_3$ with different concentrates.*